ARL-TR-8601 ● Dec 2018

US Army Research Laboratory

Software-Defined Radio Angle of Arrival Measurement of Modulated Signals

by Michael Don and Dakota Wessel

NOTICES

Disclaimers

The findings in this report are not to be construed as an official Department of the Army position unless so designated by other authorized documents.

Citation of manufacturer's or trade names does not constitute an official endorsement or approval of the use thereof.

Destroy this report when it is no longer needed. Do not return it to the originator.

ARL-TR-8601 ● DEC 2018

US Army Research Laboratory

Software-Defined Radio Angle of Arrival Measurement of Modulated Signals

by Michael Don
Weapons and Materials Research Directorate, ARL

Dakota Wessel
Drexel University, Philadelphia, PA

REPORT DOCUMENTATION PAGE

Form Approved
OMB No. 0704-0188

1. REPORT DATE *(DD-MM-YYYY)*	2. REPORT TYPE	3. DATES COVERED (From - To)
December 2018	Technical Report	March–August 2018

4. TITLE AND SUBTITLE
Software-Defined Radio Angle of Arrival Measurement of Modulated Signals

5a. CONTRACT NUMBER

5b. GRANT NUMBER

5c. PROGRAM ELEMENT NUMBER

6. AUTHOR(S)
Michael Don and Dakota Wessel

5d. PROJECT NUMBER

5e. TASK NUMBER

5f. WORK UNIT NUMBER

7. PERFORMING ORGANIZATION NAME(S) AND ADDRESS(ES)
US Army Research Laboratory
ATTN: RDRL-WML-F
Aberdeen Proving Ground, MD 21005

8. PERFORMING ORGANIZATION REPORT NUMBER
ARL-TR-8601

9. SPONSORING/MONITORING AGENCY NAME(S) AND ADDRESS(ES)

10. SPONSOR/MONITOR'S ACRONYM(S)

11. SPONSOR/MONITOR'S REPORT NUMBER(S)

12. DISTRIBUTION/AVAILABILITY STATEMENT
Approved for public release; distribution is unlimited.

13. SUPPLEMENTARY NOTES

14. ABSTRACT
The US Army Research Laboratory (ARL) is investigating localization technologies for GPS-denied environments. One such technology is RF angle of arrival (AoA). Previous research at ARL demonstrated the feasibility of RF AoA for swarm localization using continuous wave signals. This report applies this research to modulated signals, allowing for data communications as well as AoA measurement. Two modulation schemes are examined for their suitability for AoA measurement, culminating in a laboratory experiment successfully demonstrating AoA measurement with modulated signals.

15. SUBJECT TERMS
angle of arrival, software-defined radio, localization, modulation, direction finding

16. SECURITY CLASSIFICATION OF:			17. LIMITATION OF ABSTRACT	18. NUMBER OF PAGES	19a. NAME OF RESPONSIBLE PERSON
a. REPORT	b. ABSTRACT	c. THIS PAGE			Michael Don
Unclassified	Unclassified	Unclassified	UU	31	19b. TELEPHONE NUMBER (Include area code) 410-306-0775

Contents

List of Figures

List of Tables

1. Introduction

The global positioning system (GPS) is currently the backbone of the military's position, navigation, and timing infrastructure. But GPS is vulnerable to jamming and other malicious attacks,[1] necessitating the development of other localization technologies.[2] One such technology is radio frequency (RF) angle of arrival (AoA). There are various methods to calculate AoA, but frequently it is determined from the phase differences between the elements of an antenna array.[3] RF AoA has been used in the past for naval and aircraft navigation and can provide an alternative to GPS in challenging environments.[4]

Building on previous research with software-defined radio (SDR),[5,6] the US Army Research Laboratory (ARL) demonstrated RF AoA measurement of continuous wave (CW) using an SDR.[7] SDR, as the name suggests, is a radio platform where most of the functionality is defined in software instead of hardware. This makes it a flexible system for specialized applications such as AoA. SDR can be further employed to measure the AoA of modulated signals, allowing a network of agents to use the same signals for communications and angle measurements. A sinusoid can be modulated though its amplitude, frequency, and phase, resulting in amplitude modulation (AM), frequency modulation, and phase modulation. This report analyzes AoA measurement using modulated signals, exploring the suitability of modulation schemes for AoA, and demonstrating angle measurements using an SDR.

First, AoA theory is reviewed. Next, the SDR inphase/quadrature (IQ) modulation and demodulation are presented. Two modulation methods are then compared for their suitability for AoA measurement, binary phase shift keying (BPSK) and binary frequency shift keying (BFSK). AM methods are excluded from consideration because they have poor noise performance and are generally not employed alone in modern wireless communications. Finally, the results of a laboratory experiment using BFSK are presented.

2. Theory

2.1 RF AoA Measurement

The AoA of an RF signal can be determined using the system in Fig. 1.[3] A_1 and A_2 indicate the position of two antennas spaced a distance d apart. The red lines indicate the RF signal's direction of propagation from the source to the antennas. If the distance from the signal source to the antennas is much greater than d, these

lines can be assumed to be parallel. The angle of arrival, θ, is shown as the angle off center of the incoming RF signal that intersects A_2. Since $\theta + \alpha = 90°$, and $\theta + \angle PA_1A_2 = 90°$, then $\angle PA_1A_2$ is also θ. The length of $\overline{PA_2}$ is the difference in distance the RF signal must travel to A_2 as compared to A_1. Given an RF signal with wavelength λ, assuming $d \leq \lambda/2$ and $-90° \leq \theta \leq 90°$, the phase difference betwen the received signals at A_1 and A_2 is given by

$$\Delta\phi = 2\pi\left(\frac{d\sin\theta}{\lambda}\right), \tag{1}$$

where $-\pi \leq \Delta\phi \leq \pi$. Here and in the rest of this report, phases are in radians while angles are in degrees. Given a measured phase difference between A_1 and A_2, the angle of arrive is then

$$\theta = \sin^{-1}\left(\frac{\lambda\left(\frac{\Delta\phi}{2\pi}\right)}{d}\right). \tag{2}$$

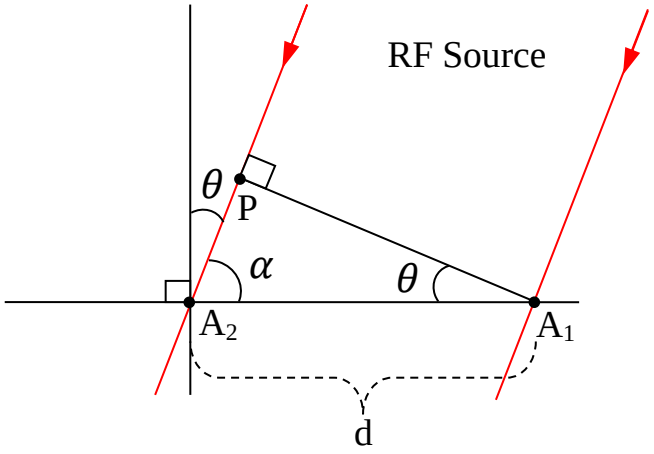

Fig. 1 AoA system with two antennas

From Eq. 1, if $d > \lambda/2$, $\Delta\phi$ can exceed the range of $-\pi \leq \Delta\phi \leq \pi$. This causes an ambiguity problem since values of $\Delta\phi$ and $\Delta\phi \pm 2\pi$ cannot be distinguished from each other at the antennas, leading to multiple solutions for θ. In order to correct this problem, an integer I can be added to Eq. 2 to account for the phase rollovers.

$$\theta = \sin^{-1}\left(\frac{\lambda\left(\frac{\Delta\phi}{2\pi}+I\right)}{d}\right). \tag{3}$$

Typically, a third antenna is used to obtain the extra information required to resolve the ambiguity.[8,9] Alternatively, another $\Delta\phi$ measurement using a different

wavelength can be used for ambiguity resolution.[7] In this report, the ambiguity problem will be ignored and it will be assumed $d \leq \lambda/2$.

The performance of AoA measurement is not constant across θ. Figure 2 shows $\Delta\phi$ as a function of θ. At larger angles, a small change in $\Delta\phi$ corresponds to a large change in θ. This makes θ more sensitive to noise at larger angles. Figure 3 shows average angle error versus angle for three levels of noise. The noise values refer to the standard deviation of Gaussian noise added to a unit amplitude input signal.

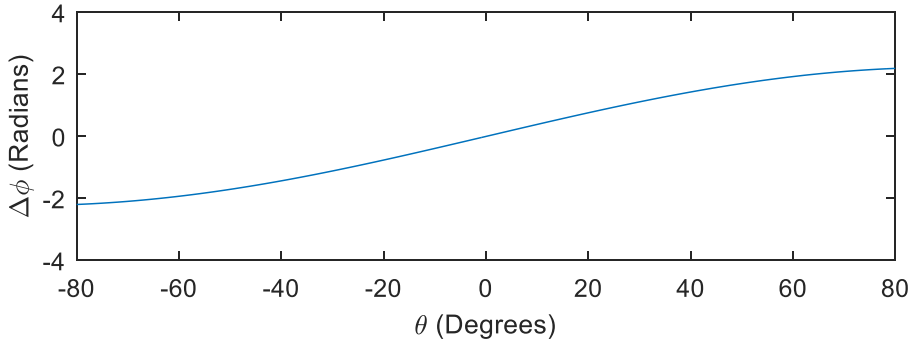

Fig. 2 $\Delta\phi$ as a function of θ

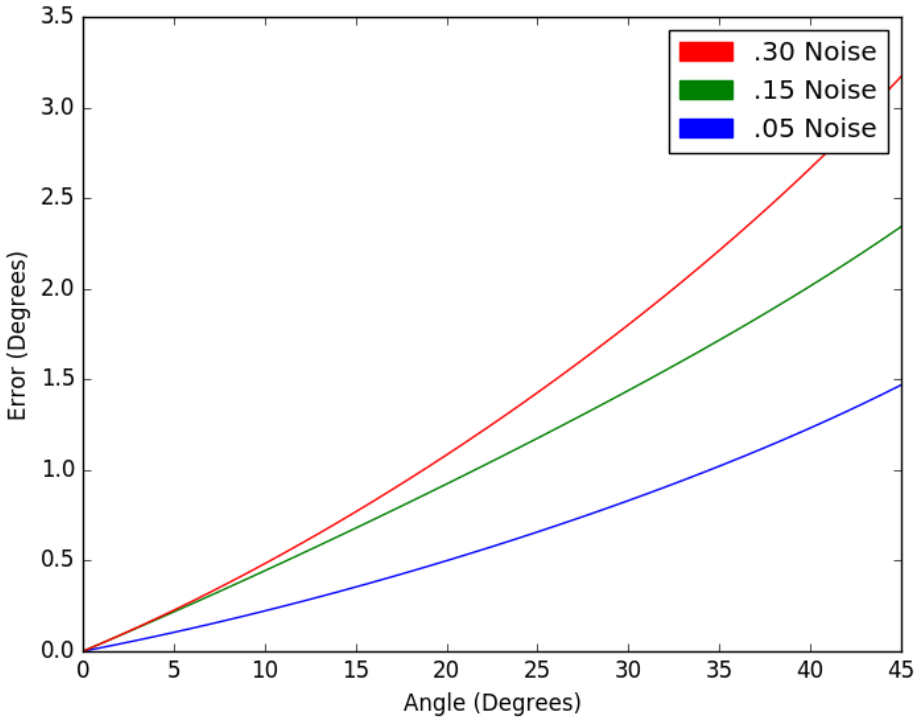

Fig. 3 AoA error as a function of angle

2.2 IQ Modulation and Demodulation

Now that AoA measurement has been reviewed, we describe how an SDR processes RF signals. In wireless communications, information is transmitted by using a modulation signal to vary a high-frequency carrier signal. Given a sinusoidal carrier of frequency f_c, information can be encoded by modulating the amplitude ($A(t)$), frequency ($f(t)$), or phase ($\varphi(t)$).

$$y(t) = A(t)\cos(2\pi\big(f_c + f(t)\big) + \varphi(t)). \tag{4}$$

SDR typically implements this modulation by reformulating Eq. 4 in terms of IQ data applied to a carrier signal (cosine) and a 90° shifted version of the carrier (sine) to produce the desired amplitude, frequency, and phase changes.

$$A(t)co\,s\left(2\pi\big(f_c + f(t)\big) + \varphi(t)\right) = I(t)\cos(2\pi f_c t) - Q(t)\sin(2\pi f_c t). \tag{5}$$

The modulation is formatted in this manner because the RF transmitter hardware outlined in Fig. 4 is relatively simple to implement.

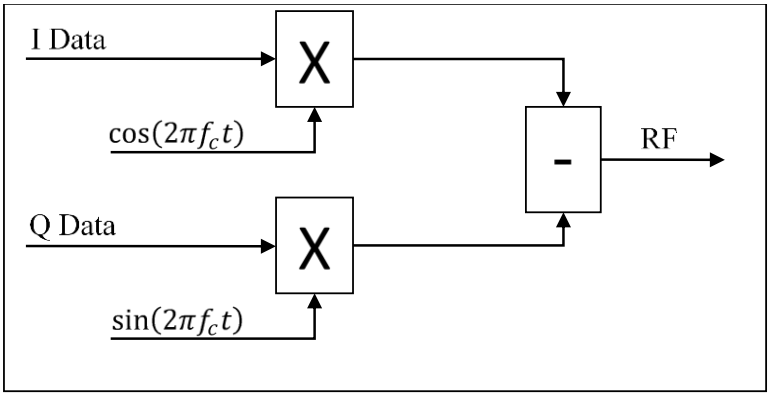

Fig. 4 IQ modulator

After the modulated signal is transmitted, it is received and demodulated to extract the encoded information. A block diagram of demodulation is shown in Fig. 5.

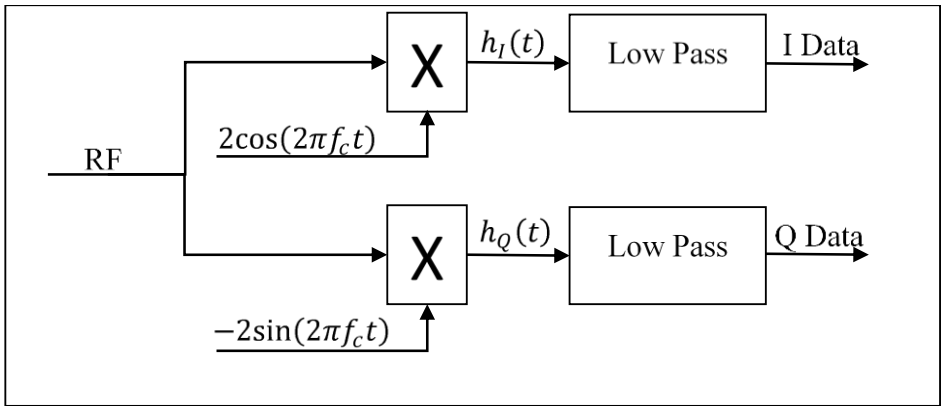

Fig. 5 IQ demodulator

Starting with the demodulation of the I data, an input RF signal formulated in terms of IQ data as in Eq. 5 gives

$$h_I(t) = 2cos(2\pi f_c t)(I(t)\cos(2\pi f_c t) - Q(t)\sin(2\pi f_c t)). \quad (6)$$

Using the double angle formulas

$$\cos^2(\theta) = \frac{\cos(2\theta) + 1}{2} \quad (7)$$

$$\sin(\theta)\cos(\theta) = \sin(2\theta), \quad (8)$$

$h_I(t)$ becomes

$$h_I(t) = I(t) + I(t)cos(4\pi f_c t) - Q(t)\sin(4\pi f_c t). \quad (9)$$

This leaves the baseband I data with additional signals at twice the carrier frequency. Filtering out these higher frequencies using a low-pass filter will restore the original I data. Similarly, for the Q data

$$h_Q(t) = -2sin(2\pi f_c t)(I(t)\cos(2\pi f_c t) - Q(t)\sin(2\pi f_c t)). \quad (10)$$

With the additional double-angle formula

$$\sin^2(\theta) = \frac{1 - \cos(2\theta)}{2}, \quad (11)$$

$h_Q(t)$ becomes

$$h_Q(t) = -I(t)sin(4\pi f_c t) + Q(t) - Q(t)\cos(4\pi f_c t). \quad (12)$$

Here the baseband Q data are left with additional high-frequency signals. Filtering out these high frequencies will restore the original Q data.

Real modulation and demodulation hardware may make use of intermediate frequencies in the conversion process of IQ data to the carrier frequency, but the basic modulation theory remains the same as outlined here.

3. Evaluation of Modulation Schemes

3.1 BPSK

BPSK is a type of modulation that encodes information in the phase of the signal.[10] Figure 6 shows binary data, IQ data, and the modulated carrier signal. A more extensive treatment of BPSK is included in Appendix A, with the source MATLAB[11] code for the plots in Appendix B. The phase changes in the modulated signal can clearly be seen to line up with the data bits. Examining the IQ data, we concluded that BPSK is not well suited to AoA measurements. As explained previously in reference to Fig. 1, AoA is calculated by comparing the phase of the received signals at the two antennas. However, SDR demodulates the BPSK signals into its original IQ data, where the Q signal is constant, and the I is binary. A constant signal certainly cannot be used to measure $\Delta\phi$, and a binary signal can only measure phase at the bit boundaries, a small minority of full signal.

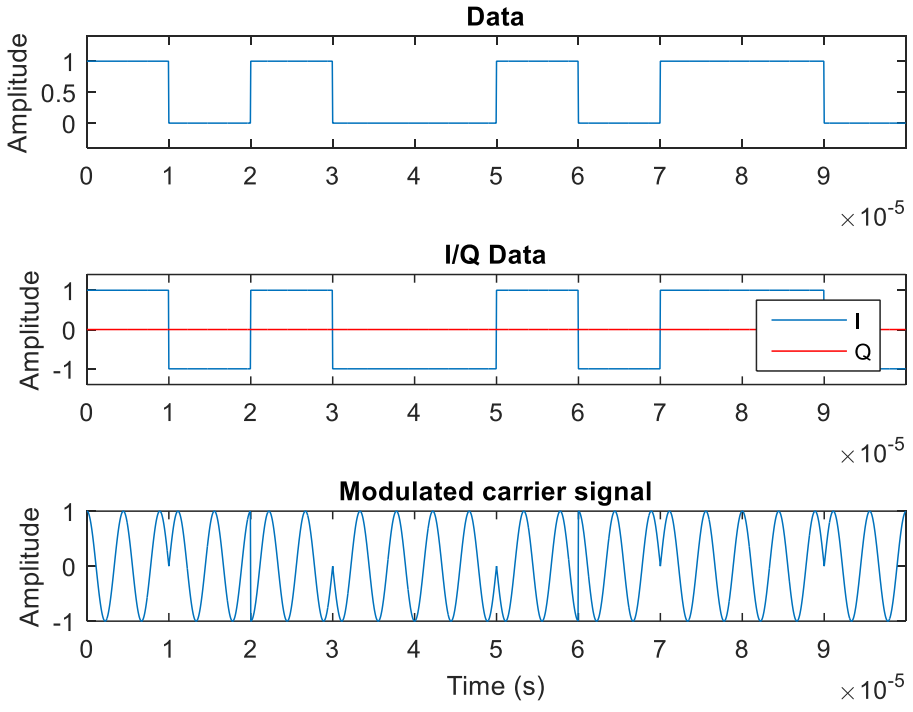

Fig. 6 BPSK modulation

3.2 BFSK

BFSK is a modulation technique that changes the frequency of a carrier signal to encode information.[10] Binary symbols 0 and 1 correspond to a frequency deviation of $+f_d$ and $-f_d$, respectively.

$$s_1(t) = \cos(2\pi t(f_c + f_d)). \tag{13}$$

$$s_0(t) = \cos(2\pi t(f_c + f_d)). \tag{14}$$

Using the angle-sum identity,

$$\cos(a + b) = \cos(a)\cos(b) - \sin(a)\sin(b). \tag{15}$$

The IQ data can be formed as follows:

$$s_1(t) = I(t)\,cos(2\pi f_c t) + Q(t)\,sin(2\pi f_c t)\,, \quad I(t) = \cos(-2\pi f_d t), \quad Q(t) = \sin(-2\pi f_d t). \tag{16}$$

$$s_0(t) = I(t)\,cos(2\pi f_c t) + Q(t)\,sin(2\pi f_c t)\,, \quad I(t) = \cos(2\pi f_d t), \quad Q(t) = \sin(2\pi f_d t). \tag{17}$$

Figure 7 shows the process of BFSK modulation. The top plot shows the data. The next plot shows the phase angle used to generate the IQ data. The phase angle is the angle of the sine and cosine terms of the IQ data in Eqs. 16 and 17. This gives the phase angle a slope of $-2\pi f_d$ for a data bit of 1, and a slope of $2\pi f_d$ for a data bit of 0. The third plot shows the IQ data itself generated from the phase angle. The last plot shows the modulated signal with higher frequencies corresponding to a 1 and lower frequencies corresponding to a 0.

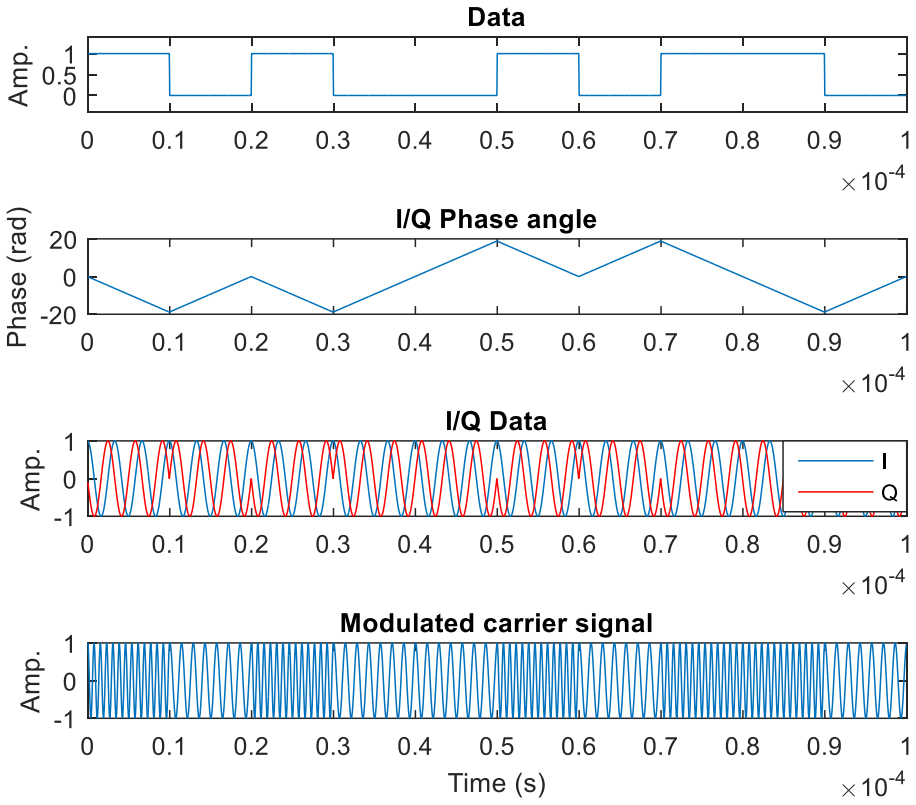

Fig. 7 BFSK modulation

Figure 8 shows the demodulation process. The top plot shows the received signal. The next plot shows the recovered IQ data. Since the I and Q data were formed from the cosine and sine of the phase angle, the phase angle can be recovered from the inverse tangent of the Q data divided by the I data.

$$\varphi(t) = tan^{-1}\left(\frac{Q(t)}{I(y)}\right). \tag{18}$$

The original data can then be extracted from the slope of the phase angle through differentiation, which is shown in the bottom plot where the recovered data overlap the original data.

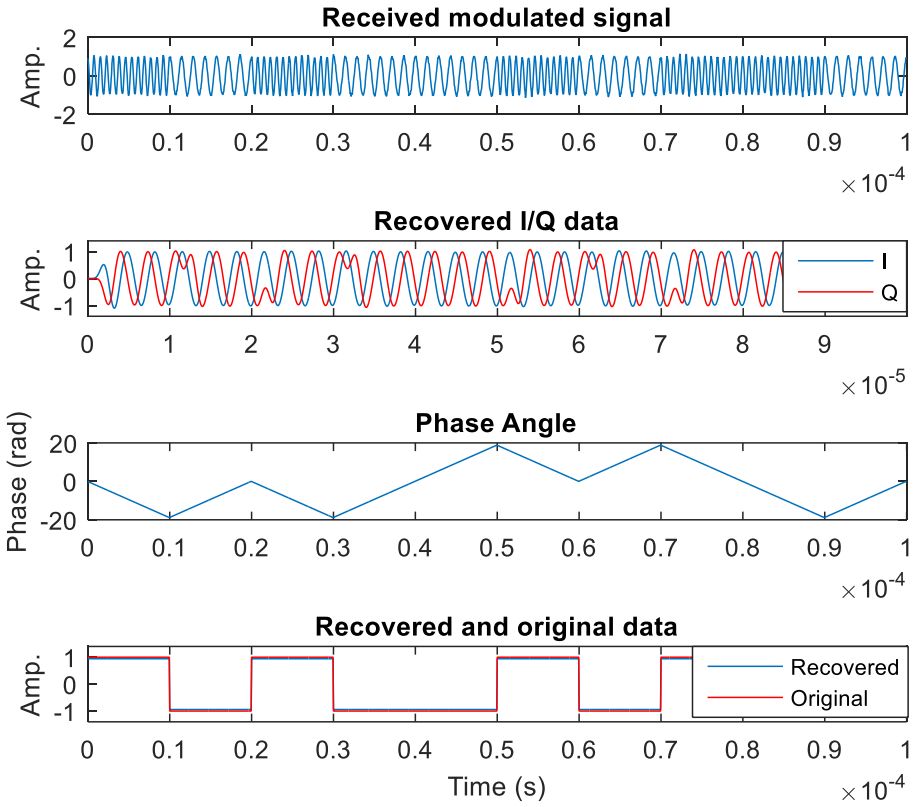

Fig. 8 BFSK demodulation

Examining the IQ data in Fig. 7, it is apparent that BFSK is well suited to AoA measurement. Both the I and Q are sinusoidal, allowing for $\Delta\phi$ to be measured. The Q data in Fig. 8, unlike the ideal Q data in Fig. 7, have more gradual phase transitions at the bit boundaries. This can cause some variability in the $\Delta\phi$ measurement, but it can be easily corrected by only using the Q data in the middle of the bits away from the boundaries.

Although AoA measurements from phase differences have been reviewed, and IQ demodulation and modulation have been presented, the relationship between $\Delta\phi$ in the IQ data and $\Delta\phi$ in the RF signals has yet to be shown. Starting with a single RF sinusoid with frequency $f_c + f_d$ given as

$$x(t) = \cos(2\pi t(f_c + f_d)), \tag{19}$$

the received signals at antennas A_1 and $A_2$are then

$$x_1(t) = \cos(2\pi t(f_c + f_d) + \phi_1) \tag{20}$$

$$x_2(t) = \cos(2\pi t(f_c + f_d) + \phi_2). \tag{21}$$

Using the cosine-sum formula

$$\cos(\alpha + \beta) = \cos\alpha \cos\beta - \sin\alpha \sin\beta, \tag{22}$$

with $\alpha = 2\pi t f_d + \phi$ and $\beta = 2\pi t f_c$, Eqs. 23 and 24 can be written as

$$x_1(t) = \cos(2\pi t f_d + \phi_1)\cos(2\pi t f_c) - \sin(2\pi t f_d + \phi_1)\sin(2\pi t f_c) \tag{23}$$

$$x_2(t) = \cos(2\pi t f_d + \phi_2)\cos(2\pi t f_c) - \sin(2\pi t f_d + \phi_2)\sin(2\pi t f_c). \tag{24}$$

This is the IQ-signal representation in Eq. 5, with $I_1(t) = \cos(2\pi t f_d + \phi_1)$ and $Q_1(t) = \sin(2\pi t f_d + \phi_1)$. ϕ_2 has an identical IQ representation. The phase can then be calculated from $I_1(t)$ or $Q_1(t)$ as

$$\frac{Q_1(t)}{I_1(t)} = \tan(2\pi t f_d + \phi_1) \tag{25}$$

$$\phi_1 = \tan^{-1}\left(\frac{Q_1(t)}{I_1(t)}\right) - 2\pi t f_d. \tag{26}$$

with identical equations for ϕ_2. This leads to a $\Delta\phi$ measurement of

$$\Delta\phi = \tan^{-1}\left(\frac{Q_1(t)}{I_1(t)}\right) - \tan^{-1}\left(\frac{Q_2(t)}{I_2(t)}\right), \tag{27}$$

where the $2\pi t f_d$ terms cancel out. Thus, the recovered IQ data preserve the phase information of the antenna signals. This proof for $f_c + f_d$ also applies to $f_c - f_d$, allowing $\Delta\phi$ to be extracted for BFSK signals. Typically, $f_d \ll f_c$, allowing a single value of λ based on f_c alone to be used for AoA calculations without any noticeable degradation of accuracy.

4. Laboratory Experiment

A laboratory experiment was conducted to demonstrate AoA measurements with modulated signals. Figure 9 shows the experiment setup. In order to avoid multipath, cables were used to simulate an AoA. A Universal Software Radio Peripheral (USRP) B200mini[12] acts as the signal source, transmitting a BFSK signal from a saved BFSK waveform file. The signal passes through a 3-ft cable to an RF splitter where it divides into two paths. The length of these paths can be used to create a phase difference in the signals. A USRP E310[13] with two receiver front ends receives and records the signals for processing.

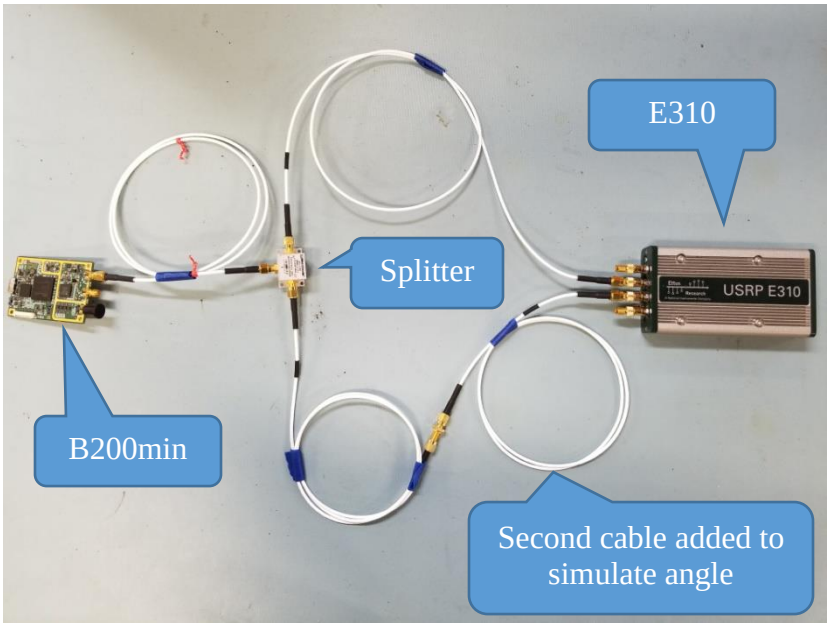

Fig. 9 AoA laboratory experiment setup

The two front ends of the E310 use separate, unsynchronized oscillators creating an unknown phase bias between the two receiver channels. Using two 3-ft cables for each transmit path, this bias was measured as 3.146 rad. A second 3-ft cable was then added to one of the transmit paths to simulate an AoA, and the bias was subtracted from the measured $\Delta\phi_{measured}$ to produce the $\Delta\phi_{cal}$ values listed in Table 1. Using Eq. 2, θ_{approx} was calculated using $d = \lambda/2$ as a suitable antenna spacing. The speed of electricity in a cable differs from the speed of light by the velocity factor of the cable. These cables have velocity factor[14] of 0.695, which was used in the wavelength calculations. The experiment was repeated for the four frequencies listed.

Table 1 AoA laboratory experiment results using a 3-ft cable length

Frequency (MHz)	$\Delta\phi_{est}$	$\Delta\phi_{cal}$	θ_{est}	θ_{approx}	θ Error
50	1.767	1.74	34.236	33.632	0.604
100	0.388	0.4734	7.108	8.667	–1.559
150	–0.99	–1.254	–18.369	–23.526	5.157
200	–0.369	–2.577	–48.937	–55.113	6.176

The first two frequencies have a very small error, while the second two measurements have a larger error. As d decreases, angle errors are magnified, so it is expected that error will increase as the d values decrease. Also, the phase bias was measured once at the beginning of the experiment before the 50-MHz test.

Phase-bias measurements between each frequency change may help to reduce error. In previous research,[7] phase-bias measurement was shown to be fairly accurate, resulting in only a 0.17° angle error. More significant sources of error probably include inaccuracies caused by cable-length measurement errors and the variability of connector components. For example, Table 2 shows the same calculations as in Table 1, but with 1 inch added to the 3-ft cable length. The extra inch may represent connector lengths and cable variability, and has significantly decreased the overall angle error. Considering these factors, the experiment results verify the theoretical results demonstrating that an SDR can measure AoA from modulated signals.

Table 2 AoA laboratory experiment results using a 3-ft-1-inch cable length

f_c (MHz)	$\Delta\phi_{est}$	$\Delta\phi_{cal}$	θ_{est}	θ_{approx}	θ Error
50	1.729	1.74	33.395	33.632	–0.237
100	0.312	0.4734	5.702	8.667	–2.965
150	–1.105	–1.254	–20.591	–23.526	2.934
200	–2.522	–2.577	–53.394	–55.113	1.719

5. Conclusion

Alternative localization technologies are critical in GPS-denied environments. RF AoA is a promising localization technology that can be integrated into small embedded form factors using SDR. This report applies previous AoA research on CW signals to modulated signals. BPSK was examined and found unsuitable for AoA measurement. BFSK was determined to be more suitable for AoA measurements, leading to a successful laboratory experiment demonstrating AoA measurement using BFSK signals. Future possible research areas include the following:

- Transition the laboratory experiment to a real-time field test
- Add more antennas to determine a 2-D AoA[15]
- Explore subspace AoA algorithms[16]
- Use AoA measurements to localize networked agents

6. References

1. Bachrach A, Prentice S, He R, Roy N. RANGE–robust autonomous navigation in GPS-denied environments. J Field Robo. 2011;28.

2. Lockspeiser JR, Don ML, Hamaoui M. Radio frequency ranging for swarm relative localization. Aberdeen Proving Ground (MD): Army Research Laboratory (US); 2017 Oct. Report No.: ARL-TR-8194.

3. Read W. Review of conventional tactical radio direction finding systems. Ottawa (Ontario): Defence Research Establishment; 1989 May.

4. Howeth LS. History of communications electronics in the United States Navy. Washington (DC): GPO; 1963.

5. Don M. A low-cost software-defined telemetry receiver. Proceedings of the 51st International Telemetering Conference; 2015 Oct 26–29; Las Vegas, NV.

6. Don M. Advances in a low-cost software-defined telemetry system. Presented at the 53rd International Telemetering Conference Proceedings; 2017 Oct; Las Vegas, NV.

7. Don ML. The feasibility of radio direction finding for swarm localization. Aberdeen Proving Ground (MD): Army Research Laboratory (US); 2017 Aug. Report No.: ARL-TR-8114.

8. Jacobs E, Ralston EW. Ambiguity resolution in interferometry. IEEE Trans Aero E Sys. 1981(6):766–80.

9. Guerin D. Passive direction finding. Worcester (MA): Worcester Polytechnic Institute; 2012 Oct 10.

10. Proakis JG, Manolakis DG. Digital signal processing: principles algorithms and applications. 4th ed. Mumbai (India): Pearson Education India; 2007.

11. MATLAB. Natick (MA): The Mathworks, Inc.; 2015 [accessed 2018 Sep 4]. www.mathworks.com.

12. USRP B200mini series data sheet. Santa Clara (CA): Ettus Research [accessed 2018 Sep 4] https://www.ettus.com/content/files/USRP_B200mini_Data_Sheet.pdf.

13. USRP E310 portable and stand-alone data sheet. Santa Clara (CA): Ettus Research [accessed2018Sep4] www.ettus.com/content/files/USRP_E310_Data sheet.pdf.

14. Cable velocity factor and loss data. Atlanta (GA): American Febo Enterprises; c1996–2018 [updated 2012 Oct 19; accessed 2018 Sep 4]. https://www.febo.com/reference/cable_data.html.

15. Doi Y, Moriya H, Ichige K, Arai H, Hayashi T, Matsuno H, Nakano M. Low-cost antenna array via antenna switching for high resolution 2-D DOA estimation. Proceedings of the 2013 IEEE Workshop on InSignal Processing Systems (SiPS); 2013 Oct 16–18; Taipei City, Taiwan. p. 83–88.

16. Krim H, Viberg M. Two decades of array signal processing research: the parametric approach. IEEE Signal Processing. 1996;13(4):67–94.

Appendix A. Binary Phase Shift Keying Modulation

Binary phase shift keying (BPSK) is a type of modulation that encodes information in the phase of the signal.[1] It uses two phases to encode binary symbols 0 and 1 into the carrier signal.

$$s_1(t) = \cos(2\pi f_c t). \tag{A-1}$$

$$s_0(t) = \cos(2\pi f_c t + \pi). \tag{A-2}$$

Since a phase shift of π is equivalent to negating the cosine, the modulated signal can be formed by setting the I data to –1 and 1 for symbols 0 and 1, respectively. The Q data are set to 0 giving

$$s_1(t) = I(t)\cos(2\pi f_c t)\,, \qquad I(t) = 1 \tag{A-3}$$

$$s_0(t) = I(t)\cos(2\pi f_c t)\,, \qquad I(t) = -1\,. \tag{A-4}$$

Example data, I and Q modulation signals, and the modulated carrier signal are shown for BPSK in Fig. A-1. Note the phase change of the carrier at each bit boundary of the data. BPSK is a simple example of modulation since the I data are essentially the same as the input data itself.

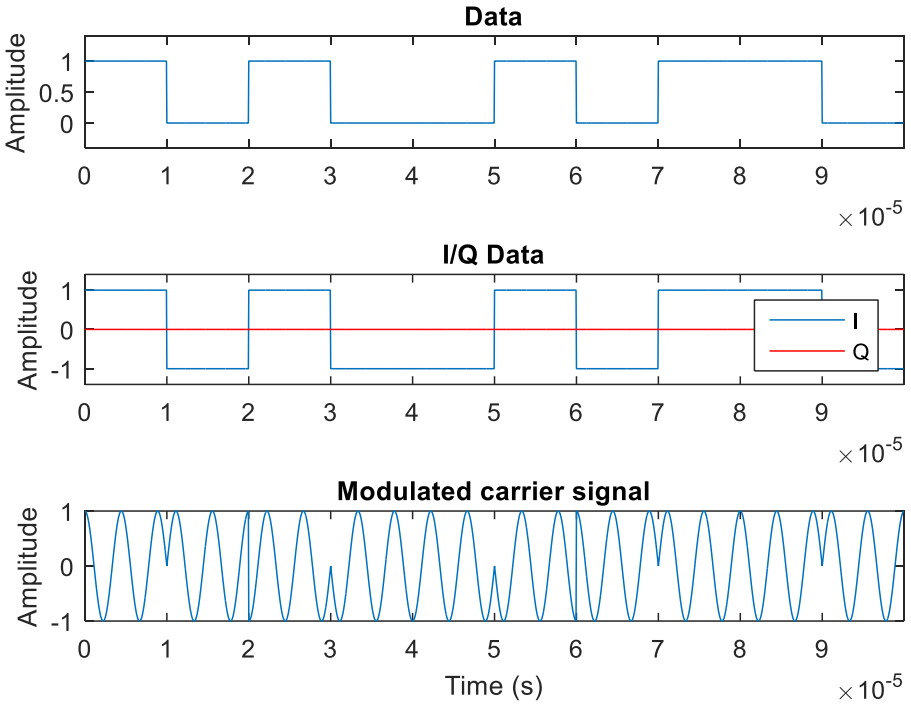

Fig. A-1 BPSK modulation (Fig. 6 in main text)

[1] Proakis JG, Manolakis DG. . Digital signal processing: principles algorithms and applications. 4th ed. Mumbai (India): Pearson Education India; 2007.

After the modulated signal is formed and transmitted, the signal is received and the original data are extracted in the demodulation process. Since the original data are equivalent to the *I* data, demodulation of BPSK is simply the process of recovering the *I* data described previously. Figure A-2 illustrates the demodulation process. The top plot shows a received modulated signal with the addition of some channel noise. The middle plot shows the received signal multiplied by a carrier signal, reintroducing the baseband and *I* data along with additional signals at twice the carrier frequency. Finally, the bottom plot shows the demodulated signal with the high frequencies filtered out. The demodulated data are distorted but clearly visible. Much of this distortion is due to the fact that the data rate and carrier frequency are relatively close. This was done so that the frequency modulation can be clearly observed. Figure A-3 shows a version of Fig. A-2 with a higher carrier frequency, resulting in much less distortion in the demodulated data.

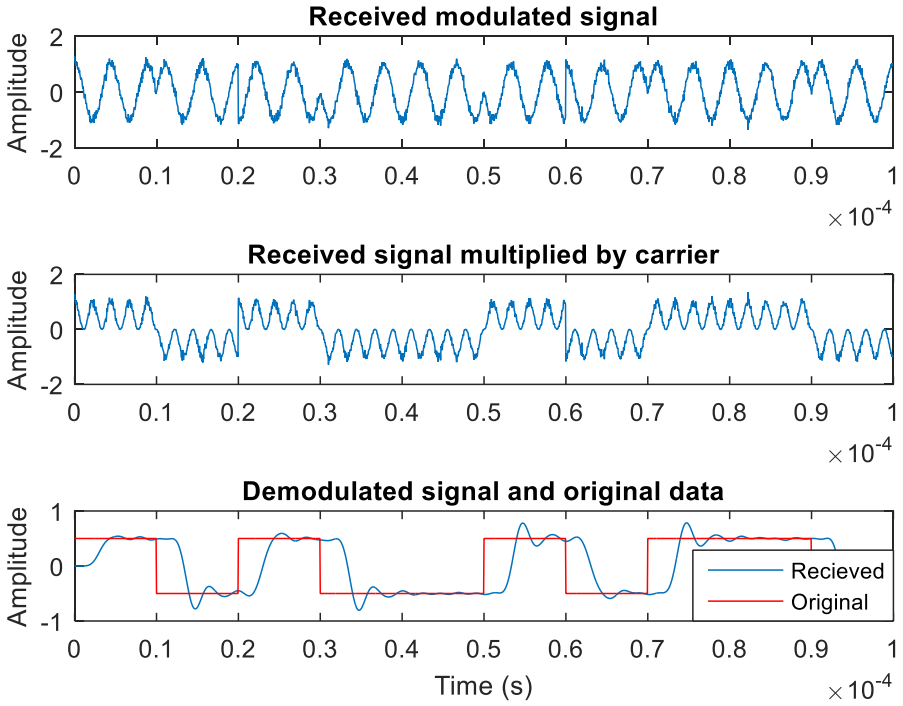

Fig. A-2 BPSK demodulation

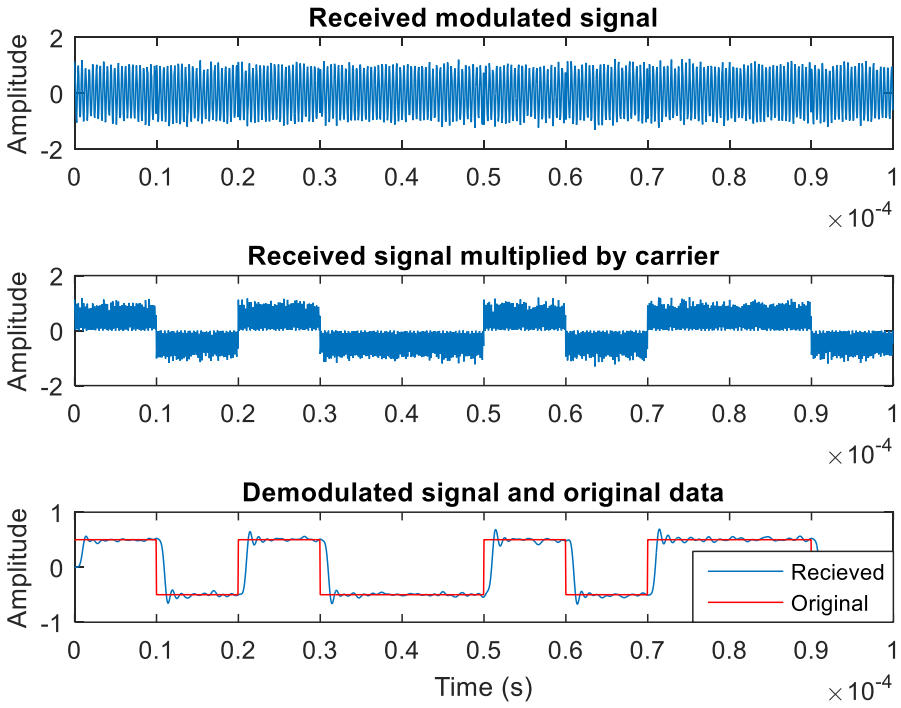

Fig. A-3 BPSK demodulation using a higher carrier frequency

Appendix B. Modulation Simulation MATLAB Code

This appendix appears in its original form, without editorial change.

bpsk.m:

```
%create data
N=10;
data=[1 0 1 0 0 1 0 1 1 0];
rate=100e3;
fc=225e3;
fs=20e6;

%upsample
samples_per_bit=fs/rate;
data_fs=ones(samples_per_bit,1)*data;
data_fs=data_fs(:);
t=((0:size(data_fs)-1)/fs)';
figure(1)
subplot(3,1,1)
plot(t,data_fs);
title('Data');
axis([0 t(end) -0.4 1.4])
xlabel('Time (s)')
ylabel('Amplitude')

%create IQ data
i=2*data_fs-1;
q=0*data_fs;
subplot(3,1,2)
plot(t,i);
hold on
plot(t,q,'r');
title('I/Q Data');
axis([0 t(end) -1.4 1.4])
xlabel('Time (s)')
ylabel('Amplitude')
legend('I','Q')
hold off

%create tx signal
fi=cos(t*2*pi*fc);
fq=sin(t*2*pi*fc);
tx=i.*fi+q.*fq;
subplot(3,1,3)
plot(t,tx);
title('Modulated carrier signal');
xlabel('Time (s)')
ylabel('Amplitude')

%channel
noise=0.1;
tx=tx+noise*randn(length(t),1);
figure(2)
subplot(3,1,1)
plot(t,tx)
title('Received modulated signal');
xlabel('Time (s)')
ylabel('Amplitude')

%demodulation
```

```
freq_error=fc*0;
phase_error=2*pi*0;
carrier=cos(t*2*pi*(fc+freq_error)+phase_error);
rx=tx.*fi;
subplot(3,1,2)
plot(t,rx)
title('Received signal multiplied by carrier');
xlabel('Time (s)')
ylabel('Amplitude')

%filter
cuttoff_freq=rate*2;
[b,a] = butter(9,cuttoff_freq/(fs/2),'low');
rx = filter(b,a,rx);
figure(2)
subplot(3,1,3)
plot(t,rx)
hold on
plot(t,data_fs-0.5,'r')
title('Demodulated signal and original data');
xlabel('Time (s)')
ylabel('Amplitude')
legend('Recieved','Original')
```

bfsk.m:

```
%create data
N=10;
data=[1 0 1 0 0 1 0 1 1 0];
rate=100e3;
fc=1e6;
fs=20e6;
fdev=300e3;  %fm deviation +/-

%upsample
samples_per_bit=fs/rate;
data_fs=ones(samples_per_bit,1)*data;
data_fs=data_fs(:);
t=((0:size(data_fs)-1)/fs)';
figure(1)
subplot(4,1,1)
plot(t,data_fs);
title('Data');
axis([0 t(end) -0.4 1.4])
xlabel('Time (s)')
ylabel('Amplitude')

%create phase angle
data_fs=data_fs*2-1;
phase=-2*pi*data_fs*fdev/fs;
phase=cumsum(phase);
subplot(4,1,2)
plot(t,phase)
title('I/Q Phase angle');
xlabel('Time (s)')
```

```
ylabel('Phase (radians)')

%create IQ data
i=cos(phase);
q=sin(phase);
subplot(4,1,3)
plot(t,i)
hold on
plot(t,q,'r')
legend('I','Q')
title('I/Q Data');
xlabel('Time (s)')
ylabel('Amplitude')
hold off

%create transmit signal
tx=i.*cos(t*2*pi*fc)+q.*sin(t*2*pi*fc);
subplot(4,1,4)
plot(t,tx)
title('Modulated carrier signal');
xlabel('Time (s)')
ylabel('Amplitude')

% Plot single-sided amplitude spectrum.
L=length(t);
y=tx;
NFFT = 2^nextpow2(L); % Next power of 2 from length of y
Y = fft(y,NFFT)/L;
f = fs/2*linspace(0,1,NFFT/2+1);
figure(2)
plot(f,2*abs(Y(1:NFFT/2+1)))
title('Single-Sided Amplitude Spectrum of TX')
xlabel('Frequency (Hz)')
ylabel('|TX|')

%channel
figure(3)
subplot(4,1,1)
noise=0.05;
tx=tx+noise*randn(length(t),1);
plot(t,tx)
title('Received modulated signal');
xlabel('Time (s)')
ylabel('Amplitude')

%recover IQ
i2=tx.*2.*cos(t*2*pi*fc);
q2=tx.*2.*sin(t*2*pi*fc);
%filter
[b,a] = butter(9,fdev*2/(fs/2),'low');
i2 = filter(b,a,i2);
q2 = filter(b,a,q2);
subplot(4,1,2)
plot(t,i2)
hold on
plot(t,q2,'r')
```

```
axis([0 t(end) -1.4 1.4])
title('Recovered I/Q data');
xlabel('Time (s)')
ylabel('Amplitude')
legend('I','Q')
hold off

%recover phase angle
rx=atan2(q,i);
rx=unwrap(rx);
figure(3)
subplot(4,1,3)
plot(t,rx)
title('Phase Angle');
xlabel('Time (s)')
ylabel('Phase (radians)')

%recover data
gain=-10;
rx=diff(rx)*gain;
subplot(4,1,4)
rx=[rx(1) rx'];
plot(t,rx)
hold on
plot(t,data_fs,'r')
xlabel('Time (s)')
ylabel('Amplitude')
title('Recovered and original data');
legend('Recovered','Original')
hold off
```

List of Symbols, Abbreviations, and Acronyms

2-D	two-dimensional
AM	amplitude modulation
AoA	angle of arrival
ARL	US Army Research Laboratory
BFSK	binary frequency shift keying
BPSK	binary phase shift keying
CW	continuous wave
GPS	global positioning system
IQ	inphase/quadrature
RF	radio frequency
SDR	software-defined radio
USRP	Universal Software Radio Peripheral

1 (PDF) DEFENSE TECHNICAL INFORMATION CTR DTIC OCA

2 (PDF) DIR ARL
IMAL HRA
RECORDS MGMT
RDRL DCL
TECH LIB

23 (PDF) DIR USARL
RDRL WML F
B ALLIK
B J ACKER
T G BROWN
S BUGGS
E BUKOWSKI
J COLLINS
J CONDON
B DAVIS
M DON
D EVERSON
R HALL
J HALLAMEYER
M HAMAOUI
T HARKINS
M ILG
B KLINE
J MALEY
C MILLER
B NELSON
D PETRICK
K PUGH
N SCHOMER
B TOPPER